CONF-890215--5

SPINODAL DECOMPOSITION OF AUSTENITE IN LONG-TERM-AGED DUPLEX STAINLESS STEEL*

CONF-890215--5

DE89 009827

H. M. Chung

Materials and Components Technology Division

Argonne National Laboratory

Argonne, Illinois 60439

February 1989

DISCLAIMER

To be presented at the Metallurgical Society Annual Meeting, February 27-March 3, 1989, Las Vegas, NV.

*Work supported by the Office of Nuclear Regulatory Research, U. S. Nuclear Regulatory Commission.

SPINODAL DECOMPOSITION OF AUSTENITE IN LONG-TERM-AGED DUPLEX STAINLESS STEEL

H. M. Chung

Materials and Components Technology Division

Argonne National Laboratory

Argonne, Illinois 60439 USA

Abstract

Spinodal decomposition of austenite phase in the cast duplex stainless steels CF-8 and -8M grades has been observed after long-term thermal aging at 400 and 350°C for 30,000 h (3.4 yr). At 320°C, the reaction was observed only at the limited region near the austenite grain boundaries. Ni segregation and "worm-holes" corresponding to the spatial microchemical fluctuations have been confirmed. The decomposition was observed only for heats containing relatively high overall Ni content (9.6-12.0 wt %) but not in low-Ni (8.0-9.4 wt %) heats. In some specimens showing a relatively advanced stage of decomposition, localized regions of austenite with a Vickers hardness of 340-430 were observed. However, the effect of austenite decomposition on the overall material toughness appears secondary for aging up to 3-5 yr in comparison with the effect of the faster spinodal decomposition in ferrite phase. The observation of the thermally driven spinodal decomposition of the austenite phase in cast duplex stainless steels validates the proposition that a miscibility gap occurs in Fe-Ni and ancillary systems.

Introduction

Cast austenitic stainless steels, composed of dual phases of austenite and ferrite, are used extensively in the nuclear, oil, and chemical industries because of their superior strength, resistance to stress corrosion cracking, weldability, and soundness of casting. In nuclear reactors, designed to operate for ~40 yr at 280-330°C, cast stainless steels are used for primary cooling pipes, valves, and pump casings, whose structural integrity of these components is vital for safe operation of the reactors. It has been known for a long time that ferritic stainless steels are susceptible to severe embrittlement when exposed to temperatures in the range of 300-500°C, owing to the precipitation of the Cr-rich α' phase. The potential for significant embrittlement of cast stainless steels has been confirmed by recent studies on cast materials that were aged at temperatures between 300 and 450°C for times up to 70,000 h (~8 yr) (1-5). Over the past several years, a number of investigations have established that α' formation by spinodal decomposition in the ferrite phase of duplex stainless steel is the primary mechanism of degradation of the material toughness after long-term thermal aging near reactor operating temperatures (i.e., 280-400°C) (6-8). The austenite phase of the duplex material has been, in general, believed to be immune to decomposition in this temperature range. However, during microstructural characterization of the duplex materials after a long-term thermal aging, spinodal-like decomposition of austenite has been observed unexpectedly in several heats of CF-8M and -8 grades. Since the duplex material is composed primarily of austenite (i.e., 60-95%), decomposition of the austenite and its possible effects on material toughness could be significant. Consequently, the austenite decomposition has been analyzed in detail by STEM, EDS, and

microhardness measurements to provide a better understanding of the reaction. The purpose of this paper is to report the results of the characterization. Since there is apparently no documented report of the spinodal decomposition of austenite under thermal aging conditions, except the findings from meteorites and material exposed to fast-neutron irradiation, the present observation of the decomposition in cast duplex stainless steels appears unique in that it was produced under thermal aging conditions.

Experimental Procedures

Several heats of cast duplex stainless steels of ASTM CF-3, -8, and -8M grades have been obtained after thermal aging at 300-400°C for up to 70,000 h (8 yr). Chemical compositions and ferrite contents of the heats are listed in Table 1. Details of the specimen geometry and size have been reported elsewhere (5). The aged specimens were examined with optical, scanning electron, and JEOL 100CX-II scanning transmission electron microscopes to characterize the microstructural evolution during the long-term thermal aging. Thin-foil specimens for TEM examination were jet thinned in an electrolytic solution of 19% ethanol, 27% butyl cellosolve, 17% perchloric acid, and 37% water by volume. The solution was maintained at -20 to -30°C during the jet thinning. EDS was conducted to determine local chemical compositions of the decomposed austenite phase of the thin-foil specimens. Vickers microhardness tests were conducted with either a 50- or 25-g load.

Results

Aged specimens obtained from the heats listed in Table 1 have been examined by TEM after long-term aging at 400, 350, and 320°C for 10,000 h (1.1 yr), 30,000 h (3.4 yr), and, in the case of Heats 278 and 280, for

70,000 h (8 yr). For Heats 47, 63, 65, and P4, austenite morphologies indicated a decomposition which occurred during aging for 30,000 h. Those heats contained a higher Ni content in the bulk specimens than the other five heats which did not show any decomposition in the austenite phase, i.e., 9.63 to 11.85 wt % vs 8.00 to 9.40%. The Ni content in austenite is 1.1 to 1.3 times higher than the bulk composition. Bright-field morphologies of the decomposed regions of austenite are shown in Fig. 1 for the four heats. Ferrite and austenite boundaries are visible in the figure for Heats 47, 63, and P4. Spinodal decomposition of ferrite, involving segregation of Fe and Cr, occurred on 0.2-0.5 nm scale, too fine to be resolvable in the figure (7,8). In the austenite grain, near the ferrite in particular, nearly spherical or elliptical regions of light contrast and several hundred nanometers in size are visible in high density. Similar regions of light contrast but of a more irregular shape are visible for Heat P4, which appears to be in a more advanced stage of decomposition than the other heats despite the lower aging temperature (i.e., 350 vs 400°C). The diffraction patterns corresponding to the decomposed regions of Fig. 1 did not show any reflections other than austenite, indicating that no other second phase is present in the austenite. The light and dark contrast in the austenite indicates an inhomogeneity in the austenite either in local chemical composition or in thickness on a fine scale, or both. Features essentially identical to those of Fig. 1 have been observed for irradiated Fe-Ni alloys and were termed as "worm-holes" (9). They apparently are caused by nonuniform chemical attack of the local region during jet thinning as a result of a nonuniform chemical composition. The "worm-hole" morphologies were observed in some but not all of the TEM specimens from each heat after identical aging. This indicates that the reaction was uneven.

Morphologies shown in Fig. 2 for Heat P4 indicate the effect of temperature on the kinetics of decomposition after aging for 30,000 h at 400, 350, and 320°C. For this particular heat, the reaction is apparently fastest at 350°C. At 320°C, the reaction was observed only on the austenite-austenite grain boundaries, Fig. 2(C). Similar morphology has been also observed in Heat 63 specimens after aging at 320°C for 30,000 h.

The specimens exhibiting a decomposition in austenite have been further analyzed by the EDS technique in SEM and STEM. For example, the decomposed austenite regions shown in the TEM micrograph of Fig. 3(A) were examined by EDS in SEM. In the SEM micrograph of Fig. 3(B), a Ni line scan is shown across the ferrite and austenite along the straight line in the middle. The Ni line scan shows a relatively flat profile in ferrite except in a few local areas that may contain the Ni- and Si-rich G phase (6,7). In contrast, the profile in austenite shows a distinctive Ni segregation. The wavelength of the Ni fluctuation in austenite is comparable to the scale of "worm-hole" separations shown in Figs. 3(D) and 2(B), i.e., ~1 μm.

The results of STEM-EDS analysis of the decomposed austenite regions are shown in Figs. 4 and 5. In Fig. 4(A), two spots (denoted with circles) were selected for EDS analysis, i.e., spots on and away from the region of light contrast. EDS profiles for the two spots are shown in Fig. 4(B) as the solid and dotted peaks (Fe, Cr, Ni, Si, and Mo peaks), respectively. Ratios for the peak heights (i.e., solid-to-dotted peak ratios) measured from Fig. 4(B) are: Fe, 0.66-0.70; Cr, 0.62; Ni, 0.62-0.63; Si, 0.67; and Mo, 0.73. This indicates a slight depletion of Ni and Cr for the lightly contrasted spot compared to the austenite matrix. This is consistent with similar observations made for the neutron irradiated Fe-Ni and Fe-Ni-Cr (9). That is,

the localized regions relatively low in Ni are preferentially attacked by the jet-thinning solution, and as a result, relatively thin local regions, and in some cases, perforations are produced [Fig. 4(A)].

In addition to the Ni-depleted lightly contrasted regions of Fig. 4, dark bands, reported to be relatively rich in Ni from the investigation of the irradiated Fe-Ni and Fe-Ni-Cr alloys (9), have been also observed in the present study. Morphology and EDS analysis of the dark bands are shown in Fig. 5. In the figure, EDS profiles from the dark band (solid bar) and from a lightly contrasted spot (dotted line) away from the dark band are compared. Ratios for the peak heights (i.e., ratio of dark band to matrix) measured from Fig. 5(B) are: Fe, 0.68; Cr, 0.75; Ni, 0.75; Si, 0.826, and Mo, 0.86. This shows that the dark bands are slightly rich in Ni and Cr, which is in contrast to the Ni-depleted nature of the lightly contrasted local regions of Fig. 4. This is again in agreement with the observation of Garner et al. (9) in which Ni-rich zones containing grain boundaries were identified in the irradiated Fe-35Ni and Fe-35Ni-7.5Cr alloys.

Selected area diffraction patterns [Fig. 5(C)] and dark-field morphology [Fig. 5(D)] of the dark bands of Fig. 5(A) indicate that they are a Ni-rich second phase which exhibits a sharp phase boundary from the austenite matrix. The diffraction pattern of Fig. 5(C) corresponds to fcc (or slightly tetragonal) FeNi structure of which lattice spacing is nearly identical to that of austenite. In the ordered state of the FeNi structure, planes of Fe and Ni atoms alternate in C-axis in unit cell, and, as a result, superlattice reflections are expected in addition to the usual austenite reflections. The structure factor F for reciprocal lattice (hkl) of the ordered structure is given by:

$F = 0$, for mixed hk

$F = 2\ (f_{Fe} + f_{Ni})$, for unmixed hk*l*

$F = 2\ (f_{Fe} - f_{Ni})$, for even hk and odd *l*, or odd hk and even *l*,

where f_{Fe} and f_{Ni} are the Fe and Ni atomic scattering factors. Apparently, the superlattice reflections are not intense enough in Fig. 5(C) to be visible, indicating that the structure $Fe_{1+x}Ni_{1-x}$ is only partially ordered at best. The invisible superlattice reflections may be also due to the very close values of f_{Fe} and f_{Ni}. A fully ordered FeNi structure has been reported for Santa Catharina meteorite whose composition is close to Fe-35Ni-0.2P in wt % (11, 12). It appears that the formation of a fully ordered stoichiometric FeNi structure is difficult in the present duplex stainless steels in which the austenite Ni content is rather low, i.e., 12-15 wt %.

Discussion

The results of TEM and EDS analyses suggest that the reaction in austenite is a spinodal decomposition involving Fe and Ni segregation. Morphology and microchemical nature of the "worm-holes" are strikingly similar to those reported for the "spinodal-like" decomposition (9, 10). The "spinodal-like" decomposition has been reported for irradiated Fe-Ni and Fe-Ni-Cr alloys, i.e., after irradiation by neutrons, ions, and electrons. However, the existence of thermally driven spinodal decomposition in the Fe-Ni and its ancillary systems has been not well established. In a series of investigations of the physical properties of Fe-Ni system, however, Tanji et al. (13-16) proposed that there is sufficient cause to suspect that a very sluggish miscibility gap occurs. Their investigation of magnetic behavior,

elastic moduli, thermoelectric power, resistivity, and interdiffusion coefficients indicated a critical temperature of ~1000°C at ~35% Ni. In the analysis of the "spinodal-like" decomposition of the irradiated materials, Garner et al. noted that the wavelength of the Fe-Ni segregation was relatively insensitive to the displacement rate (9). Since radiation-induced segregation processes are generally very sensitive to displacement rate, they argued that radiation-induced segregation is not the sole cause of the decomposition and that the Fe-Ni system has an inherent tendency toward spinodal decomposition. The present observation of the decomposition of the austenite phase in the CF-8 and -8M grade cast duplex stainless steels appears unique in that it was produced under thermal aging conditions without irradiation. The results appear to validate the propositions of Tanji et al. and Garner et al. It is likely that the decomposition process was accelerated in comparison with Fe-Ni or Fe-Ni-Cr alloys because of the presence of Mo and other alloying and impurity elements (Table 1) which tend to enhance interdiffusion by orders of magnitude.

Decomposition reported for Fe-Ni meteorites, considered to have occurred during slow cooling over millions of years, showed a Ni-rich FeNi ordered phase and Ni-depleted domains (11, 12). Wavelengths associated with the domain separation, however, appear to be an order of magnitude larger than the wavelength of spatial compositional fluctuation of Figs. 1-3, i.e., 10 vs 0.5-1 μm. In this respect, it is not clear how the decomposed structures of the meteorite and the duplex stainless steels are associated. However, a comparison of several morphologies of the decomposed structure suggests that the size and wavelength of the Ni-rich and Ni-depleted domains increase as the decomposition advances. For instance, the structure of Fig. 1(D) appears to

correspond to a more advanced stage of decomposition than Fig. 1(C). The formation of the Ni-rich partially ordered fcc (or slightly tetragonal) phase in the dark bands of Fig. 5(D) is interesting. It appears that for a higher Ni content and after a longer aging time, the phase tends toward an ordered FeNi structure, similar to that of the Santa Catharina meteorite. In these respects, it seems that the present observation and the meteorite decomposition are essentially identical regarding a thermally driven spinodal decomposition, but they represent a relatively early and a more advanced stage of decomposition, respectively.

In its advanced stage, the spinodal decomposition of austenite is expected to harden the material as in the case of the Fe-Cr decomposition of ferrite. A microhardness test was conducted on the austenite of the specimen of Fig. 2(B) and the result is shown in Fig. 6. Most of the austenite regions of the specimen showed a Vickers hardness of 160-200, which is expected for normal austenite. This is shown in Fig. 6(A). However, for a limited number of local regions, an austenitic of hardness of 340-430 was observed. A region similar to a hardened island surrounded by soft austenite is shown in Fig. 6(B). The hardened region of austenite was ~15 μm in size and much larger than the ferrite islands shown in the figure. It also appears that the chemical etching characteristics of the hardened regions are different from the normal austenite. It seems that only localized regions of the austenite reached an advanced stage of the spinodal decomposition in Fig. 6, resulting in a localized hardening of the material. TEM and EDS analyses of the localized hardened region could not be conducted. Whether ordered FeNi phase is associated with the hardened region, as in the case of the meteorite decomposition, is not clear.

Despite the localized hardening of the austenite, the overall material toughness of the specimen of Fig. 6 did not show excessive degradation in comparison with other heats of similar compositions for similar aging conditions. This is probably because the overall embrittlement was influenced primarily by the faster spinodal decomposition of ferrite and the austenite decomposition did not advance to produce a significant amount of hardened regions in the austenite. The specimen of Figs. 1(D) and 6 was apparently an advanced stage of decomposition, and yet showed a room temperature impact energy of 55-70 J/cm^2. This is within the range of values expected for similar aging conditions for other heats in which austenite decomposition was absent (5).

The aging produced at the time and temperature for the most advanced decomposition (i.e., Heat P4 aged at 350°C for 30,000 h) can be compared with the aging expected near the end-of-life reactor operation. This requires information on activation energy of the austenite decomposition near the temperature range of extrapolation. Since the information is not available, a value of ~50 kcal/mole was assumed, i.e., a value similar to the activation energy of spinodal decomposition of ferritic Fe-Cr alloys. In Fig. 7, extrapolations of the aging conditions of Fig. 2 were made to reactor operating temperatures of 320 and 280°C. Assuming an activation energy of 50 kcal/mole, a decomposition similar to that of Fig. 2(B) would be expected for aging at 320°C for 23 yr. The end-of-life aging (i.e., 32 yr at 320°C) would correspond to an aging at 350°C for 42,000 h (4.8 yr).

At this time, it is difficult to predict how significant austenite decomposition might be in relation to the overall material toughness at the end-of-life or life-extension situations for nuclear reactors. It seems

important to gain a better understanding of the nature of the localized embrittlement (Fig. 6). If the embrittlement is associated with the formation of an FeNi ordered phase, as in the case of the findings in meteorites, and the rest of Ni-depleted zone in austenite is ductile, an equilibrium volume fraction of the embrittled zone in austenite can be calculated on the basis of the Ni content of the austenite. Information to be obtained from specimens aged for longer times (e.g., 50,000 h) will be helpful to understand the end-of-life material performance.

Conclusions

1. Spinodal decomposition of austenite phase in cast duplex stainless steels CF-8 and -8M grades has been observed after long-term thermal aging at 400 and 350°C for 30,000 h (3.4 yr). At 320°C, the reaction was observed only at the limited region near the austenite grain boundaries. Ni segregation and "worm-holes" corresponding to the spatial microchemical fluctuations have been confirmed. This shows the existence of a miscibility gap in the austenite phase of the duplex material. The decomposition was observed only for heats containing relatively high overall Ni contents (9.6-12.0 wt %) but not in low-Ni (8.0-9.4 wt %) heats.

2. In some specimens showing a relatively advanced stage of decomposition, localized regions of austenite had a Vickers hardness of 340-430. However, the effect of the austenite decomposition on the overall material toughness appears secondary in comparison with the effect of the faster spinodal decomposition in ferrite phase for aging up to 3-5 yr. Effects on the material toughness after longer-term aging for end-of-life

or life-extension situations of reactors are difficult to predict at this time.

3. Present observation of the thermally driven spinodal decomposition of the austenite phase in cast duplex stainless steels validates the proposition that a miscibility gap occurs in Fe-Ni and ancillary systems.

Acknowledgements

This work was supported by the Office of Nuclear Regulatory Research, U. S. Nuclear Regulatory Commission. The author is grateful to A. Trautwein and W. Gysel of the Georg Fischer Company of Switzerland, and O. K. Chopra of Argonne National Laboratory for their efforts in making the long-term-aged specimens available for this work, and to R. A. Conner, Jr. and A. Philippides for their experimental contributions. The author also wishes to thank J. Muscara, W. J. Shack, and T. F. Kassner for helpful discussions.

References

1. A. Trautwein and W. Gysel, "Influence of Long Time Aging of CF-8 and CF-8M Cast Steel at Temperatures between 300 and 500°C on the Impact Toughness and the Structure Properties," Stainless Steel Castings, V. G. Behal and A. S. Melilli, eds., ASTM STM 756, p. 165 (1982).

2. G. Slama, P. Petrequin, and T. Mager, "Effect of Aging on Mechanical Properties of Austenitic Stainless Steel Castings and Welds," in Proc. SMIRT Post-Conference Seminar 6, Assuring Structural Integrity of Steel Reactor Pressure Boundary Components, August 29-30, 1983, Monterey, CA.

3. E. I. Landerman and W. H. Bamford, "Fracture Toughness and Fatigue Characteristics of Centrifugally Cast Type 316 Stainless Steel Pipe after Simulated Thermal Service Conditions, Ductility, and Toughness Considerations in Elevated Temperature Service," ASME MPC-8, American Society of Mechanical Engineers, 1978, p. 99.

4. K. N. Akhurst and P. H. Pumphrey, "The Aging Kinetics of CF-3 Cast Stainless Steel in the Temperature Range 300°C to 400°C," RD/L/3354/R88, Central Electricity Generating Board Research Laboratories, United Kingdom, November 1988.

5. O. K. Chopra and H. M. Chung, "Aging Degradation of Cast Stainless Steels: Effects on Mechanical Properties," in Proc. Third International Symposium on Environmental Degradation of Materials in Nuclear Power Systems-Water Reactors, August 30-September 3, 1987, Traverse City, MI, G. J. Theus and J. R. Weeks, eds., the Metallurgical Society, 1988, pp. 737-748.

6. M. K. Miller and J. Bentley, ibid., pp. 341-349.

7. H. M. Chung and O. K. Chopra, ibid., pp. 359-370.

8. J. M. Sassen, M. G. Hetherington, T. J. Godfrey, G. D. W. Smith, P. H. Pumphrey, and K. N. Akhurst, "Kinetics of Spinodal Reaction in Ferrite Phase of a Duplex Stainless Steel," ASME MPC-26, American Society of Mechanical Engineers, 1987, pp. 65-78.

9. F. A. Garner, H. R. Brager, and J. N. McCarthy, "Neutron-induced Spinodal-like Decomposition of Fe-Ni and Fe-Ni-Cr Alloys, Radiation-induced Changes in Microstructure: 13th Intl. Symp. (Part I), ASTM STP

955, F. A. Garner, N. H. Packan, and A. S. Kumar, eds., Am. Soc. for Testing and Mater., Philadelphia, 1987, pp. 775-787.

10. R. A. Dodd, F. A. Garner, J.-J. Kai, T. Lauritzen, and W. G. Johnston, "Spinodal-like Decomposition and Swelling Induced by Ion Irradiation in Simple Fe-Ni and Fe-Ni-Cr Alloys," ibid., pp. 788-804.

11. J. Danon, R. B. Scorzelli, I. Souza Azevedo, W. Curvello, J. F. Albertsen, and J. N. Knudsen, Nature 277 (1979), 284.

12. R. B. Scorzelli and J. Danon, Physica Scripta 32 (1985), 143.

13. Y. Tanji, H. Morita, and Y. Nakagawa, J. Phys. Soc. of Japan, 45, (1978), 1244.

14. Y. Tanji, Y. Nakagawa, Y. Saito, K. Nishimura, and K. Nakatsuka, Physica Status Solidi A, (1979), 513.

15. Y. Nakagawa, Y. Tanji, H. Morita, H. Hiroyoshi, and H. Fujiimori, J. of Magnetism and Magnetic Mater. 10 (1979), 145

16. Y. Tanji, Y. Nakagawa, and S. Steinemann, Physica B + C, 119 (1983), 109

Table 1. Chemical Compositions of Several Heats of CF-3, CF-8, and CF-8M Grade Cast Duplex Stainless Steels Selected for Characterization of Austenite Decomposition

Heat No.	Grade	Composition (wt %) Mn	Si	Mo	Cr	Ni	N	C	Ferrite Content (%)	Austenite Decomposition Observed[a]
47	CF-3	0.60	1.06	0.59	19.81	10.63	0.028	0.018	16.3	Yes
56	CF-8	0.60	1.16	0.30	19.33	8.93	0.030	0.060	10.1	No
59	CF-8	0.60	1.08	0.32	20.33	9.34	0.045	0.062	13.5	No
63	CF-8M	0.61	0.58	2.57	19.37	11.85	0.031	0.055	10.4	Yes
P4	CF-8M	1.07	1.02	2.05	19.64	10.00	0.151	0.040	10.4	Yes
64	CF-8M	0.60	0.63	2.46	20.76	9.40	0.038	0.038	28.4	No
65	CF-8M	0.50	0.48	2.57	20.78	9.63	0.064	0.049	23.4	Yes
278[b]	CF-8	0.28	1.00	0.13	20.20	8.27	0.027	0.038	15.0	No[c]
280[b]	CF-8	0.50	1.37	0.25	21.60	8.00	0.029	0.028	38.0	No[c]

[a]After thermal aging at 400, 350, and 320°C for 30,000 h (3.4 yr).

[b]Obtained from G. Fischer Co. of Switzerland.

[c]After aging at 400, 350, and 300°C for 70,000 h (8 yr).

Fig. 1. TEM Bright-Field Morphologies of Decomposed Austenite of Cast Duplex Stainless Steels after Aging for 30,000 h (3.4 yr). (A) Heat 47, 400°C; (B) Heat 63, 400°C; (C) Heat 65, 400°C; and (D) Heat P4, 350°C.

Fig. 2. TEM Bright-Field Morphologies of the Spinodal Decomposition of Austenite of Heat P4 after Aging for 30,000 h at (A) 400°C, (B) 350°C, and (C) 320°C.

Fig. 3. SEM-EDS Line Scan of Ni Across the Ferrite and Austenite of Heat P4 Aged at 350°C for 30,000 h Showing Local Ni Fluctuation on a Scale of ~1 μm (B). TEM bright-field image of the same region is shown in (A) for comparison.

Fig. 4. STEM-EDS Profiles (B) Obtained from the Two Circled Spots on (EDS Signal, Solid Peaks) and Away from (EDS Signal, Dotted) the Linear Feature of Light Contrast Shown in Bright-Field Image of (A). EDS profiles are magnified at bottom.

Fig. 5. STEM-EDS Profiles (B) Obtained from the Two Circled Spots (A) on the Dark Band (EDS Signal, Solid Bar) and on the Lightly Contrasted Region Away from the Dark Band (EDS Signal, Dotted). SAD pattern of (A) and a dark-field image of the band produced with the arrowed reflection of (C), are shown in (C) and (D), respectively.

Fig. 6. Microhardness Indentations on the Austenite Phase of Heat P4, Aged at 350°C for 30,000 h, Showing Normal Vickers Hardness of 160-200 in (A) and Localized Hardened Region (Vickers Hardness 340-430) Surrounded by Soft Austenite in (B).

Fig. 7. Time-Temperature Arrhenius-Plot Comparison of the Aging Conditions of the Decomposed Austenite of Heat P4 (3.4 yr at 400 and 350°C) and End-of-Life Reactor Components (32 yr at 320-280°C). Solid and broken lines represent activation energies of aging of 50 and 20 kcal/mole, respectively.

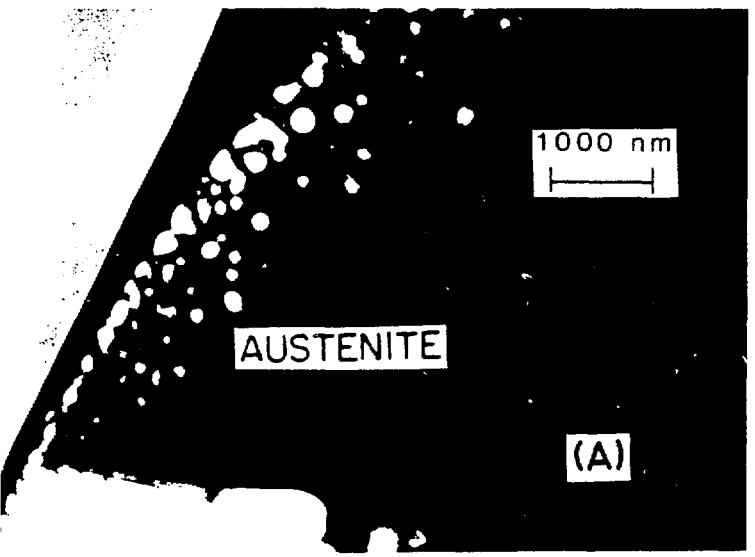
1000 nm
AUSTENITE
(A)

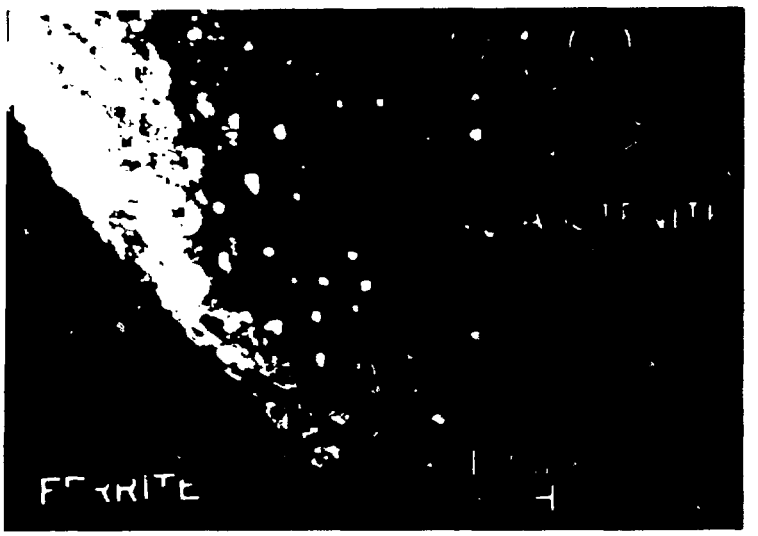
FERRITE

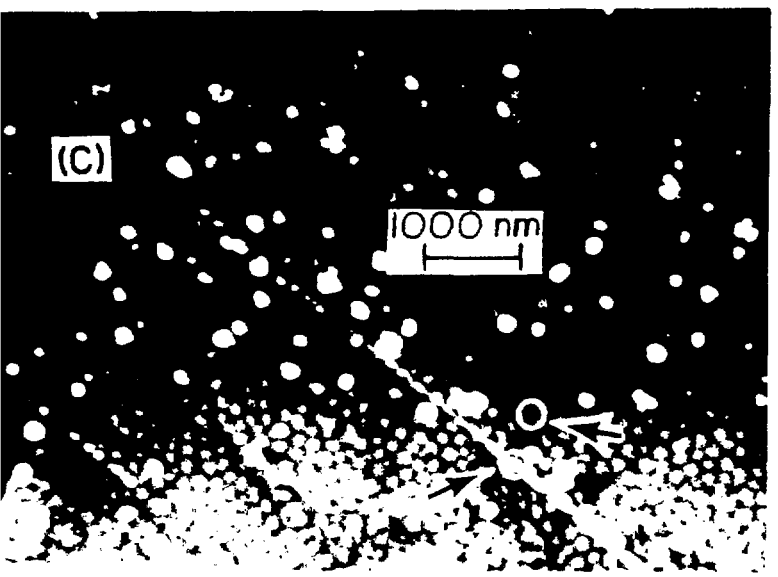
(C)
1000 nm


AUSTENITE
(D)
FERRITE

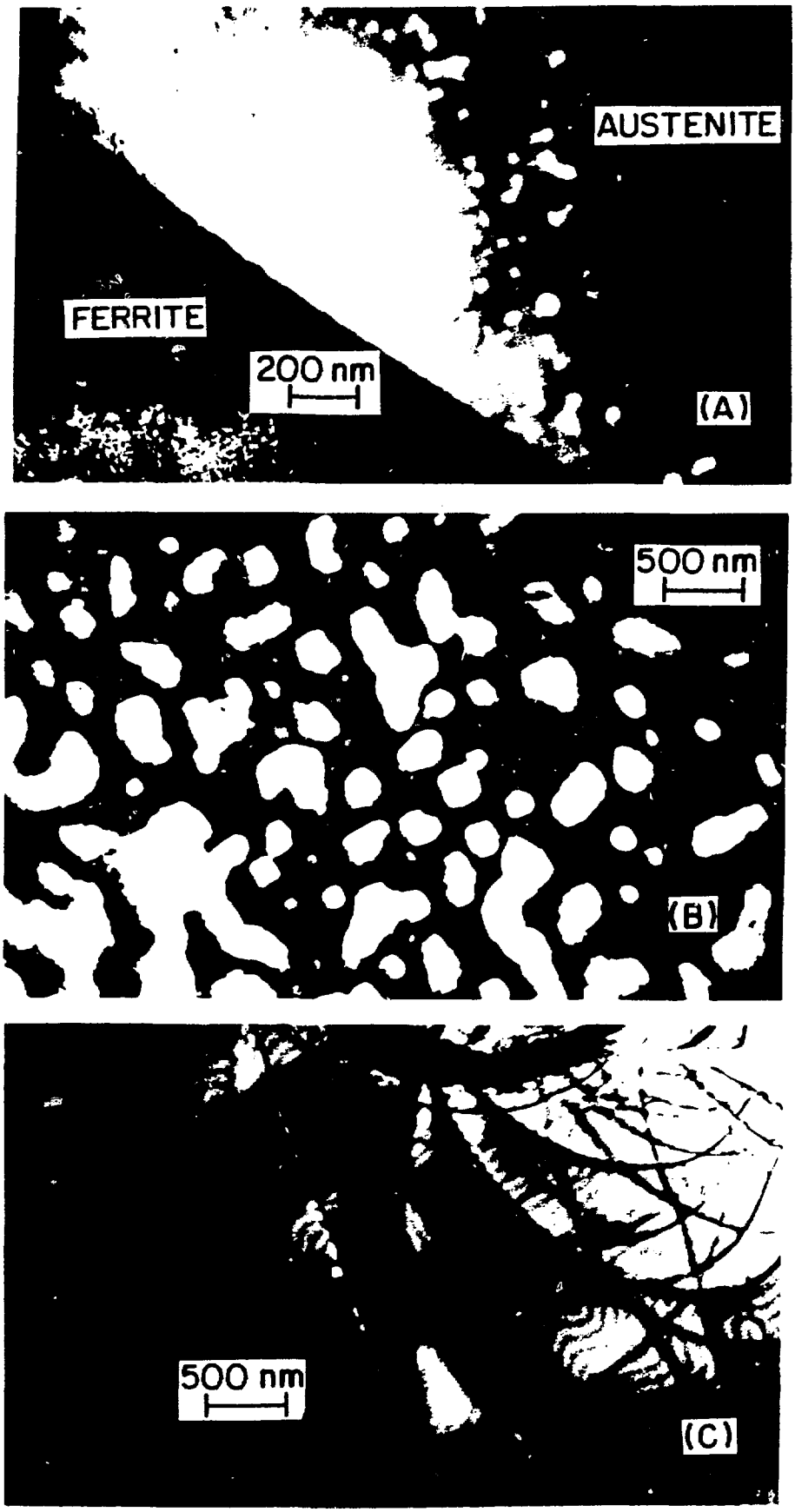

TEM Morphology of the Spinodal-Like Decomposition of Heat P4 in Austenite After Aging for 30,000h at (A) 400C, (B) 350C, and (C) 320C.

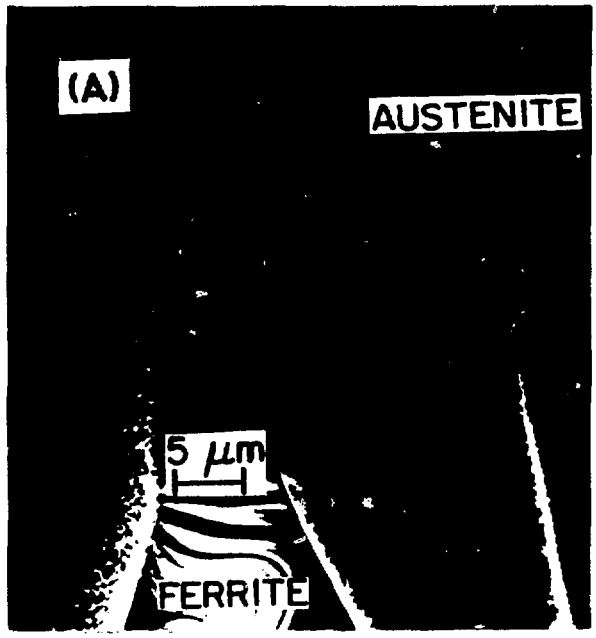
(A)
AUSTENITE
5 μm
FERRITE

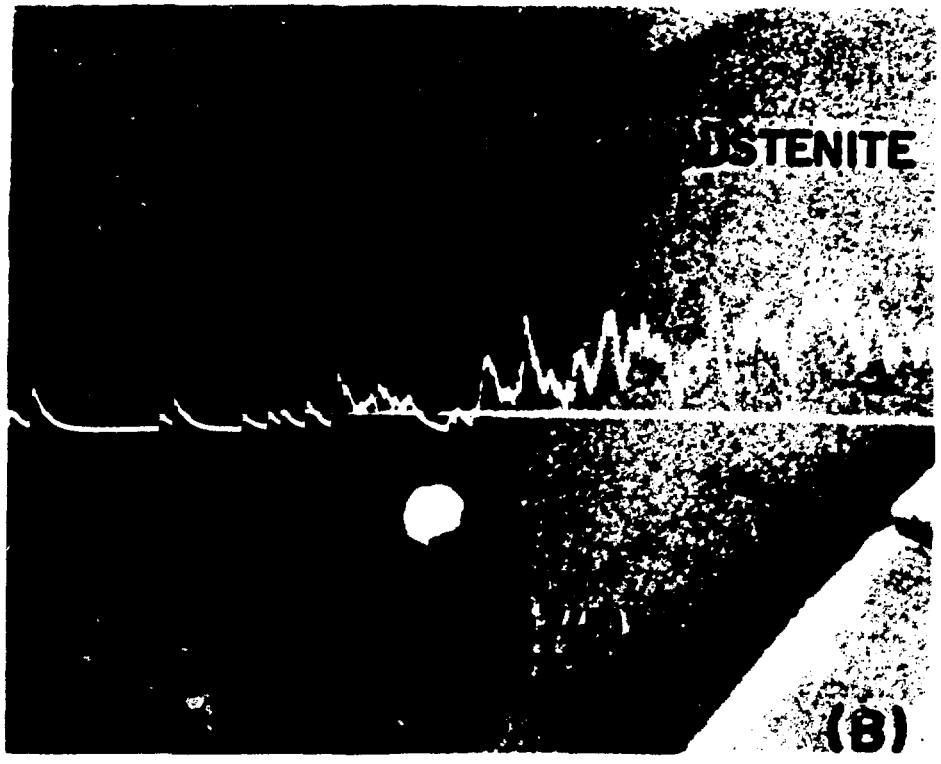
(B)

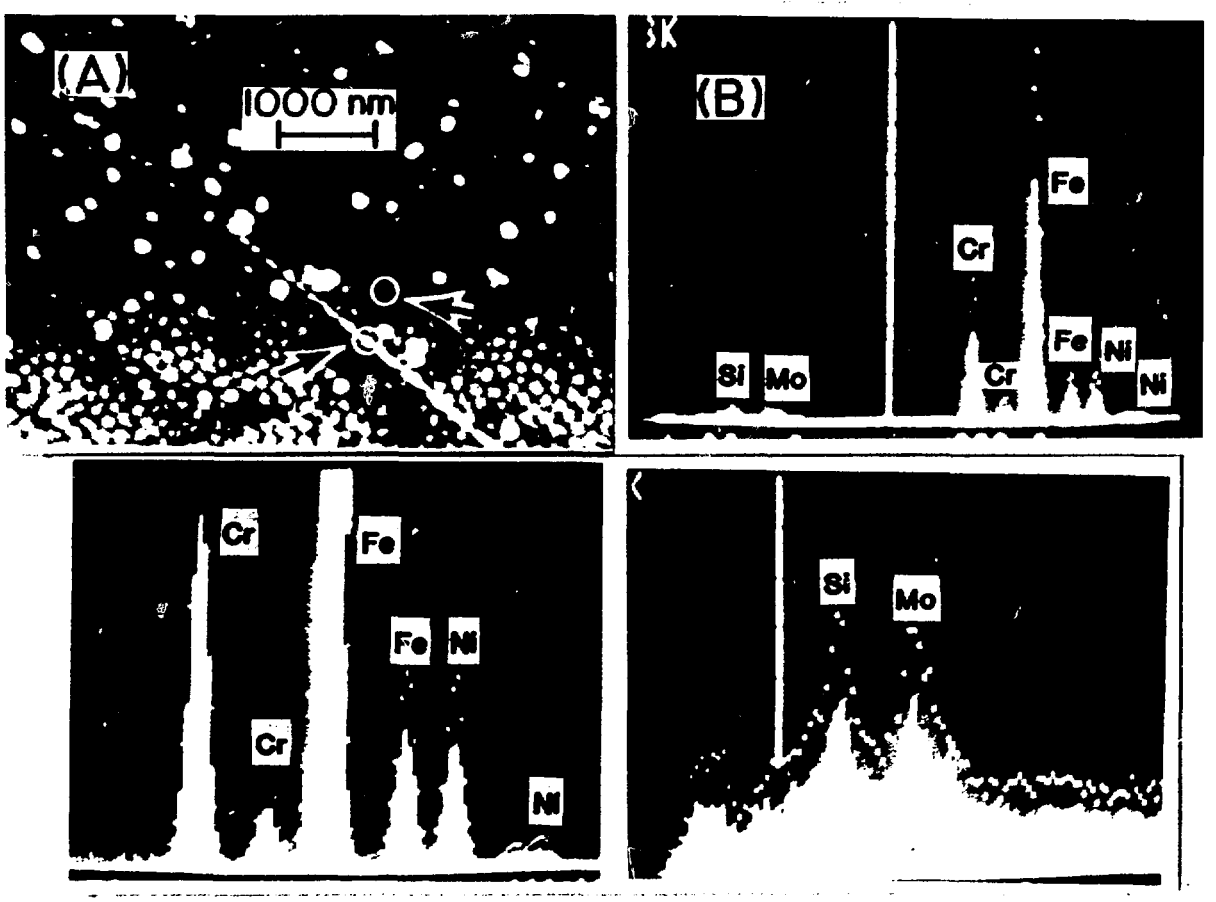
(A)
1000 nm
(B)
Si
Mo
Cr
Fe
Ni
Cr
Fe
Ni
Cr
Fe
Ni
Cr
Ni
Si
Mo

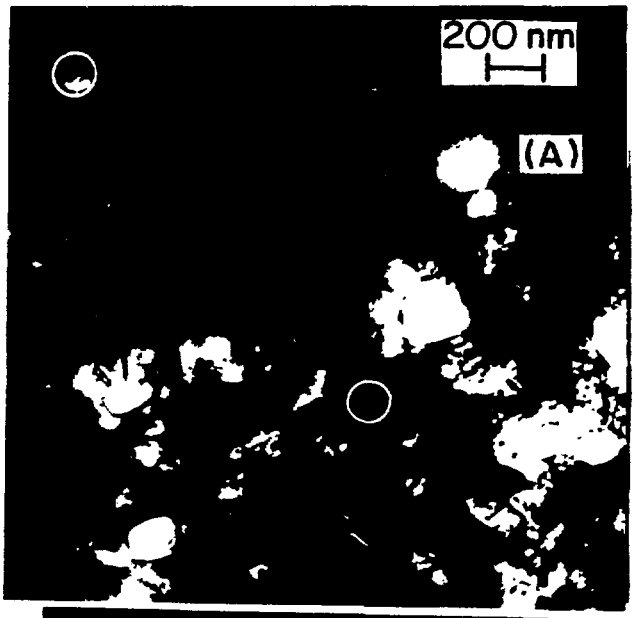
200 nm
(A)

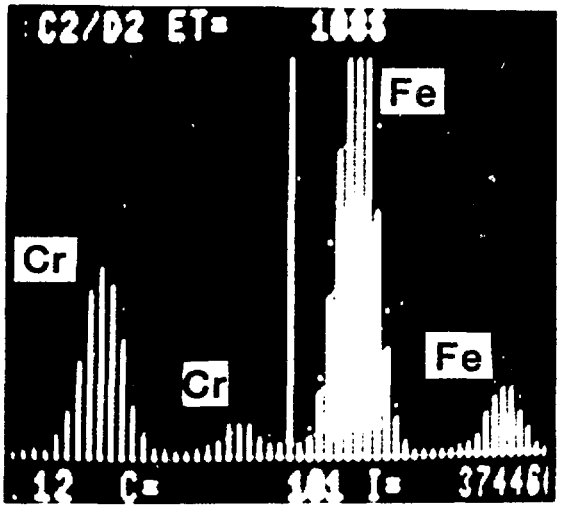
C2/D2 ET=
Fe
Cr
Cr
Fe

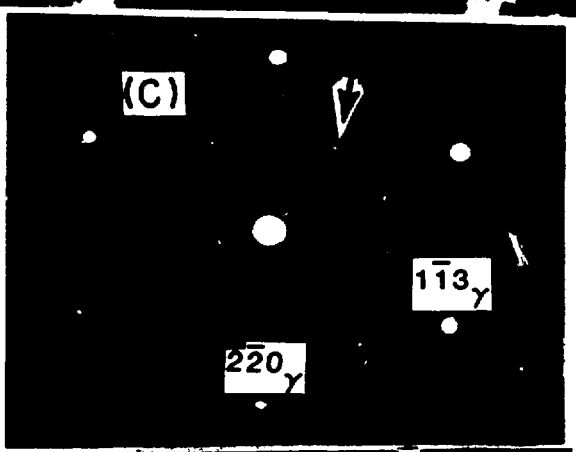
(C)
$1\bar{1}3_\gamma$
$2\bar{2}0_\gamma$

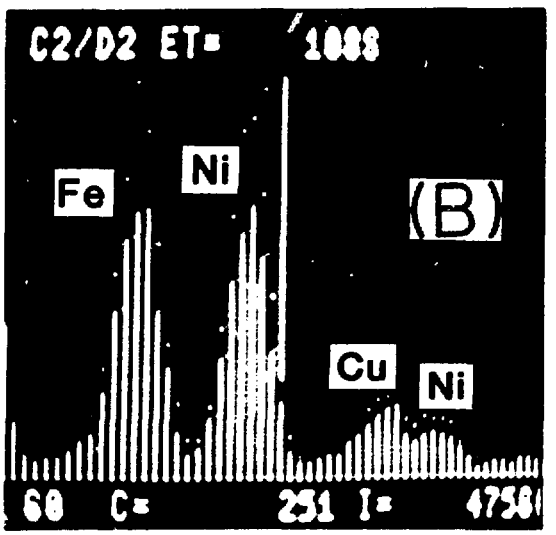
C2/D2 ET=
Fe
Ni
(B)
Cu
Ni

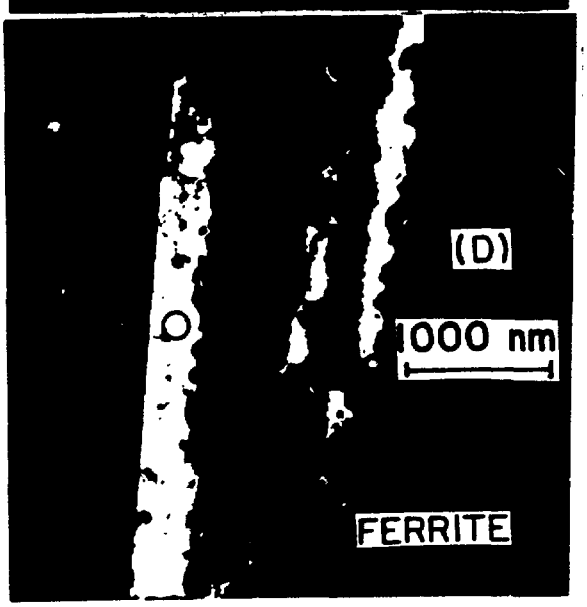
(D)
1000 nm
FERRITE

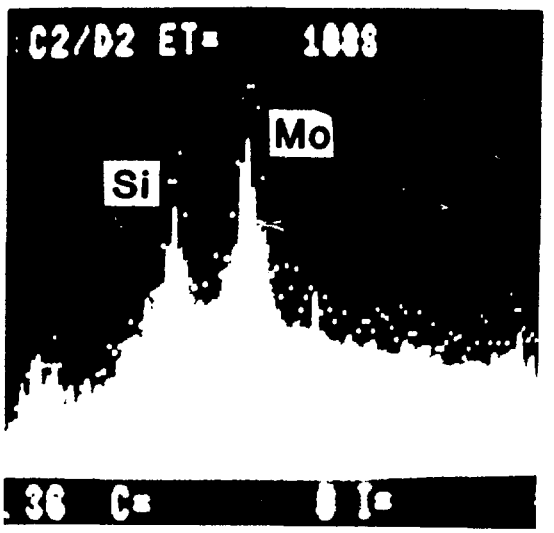
C2/D2 ET=
Mo
Si

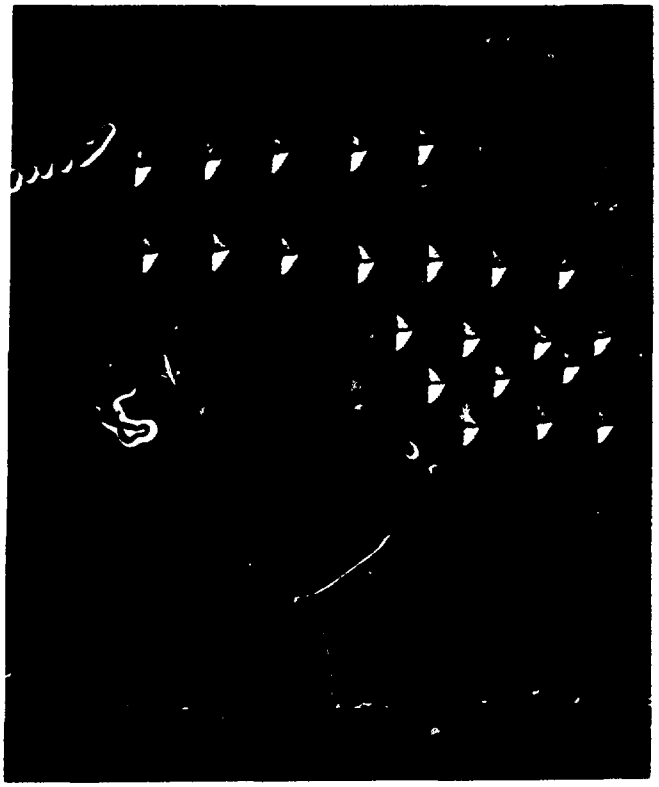

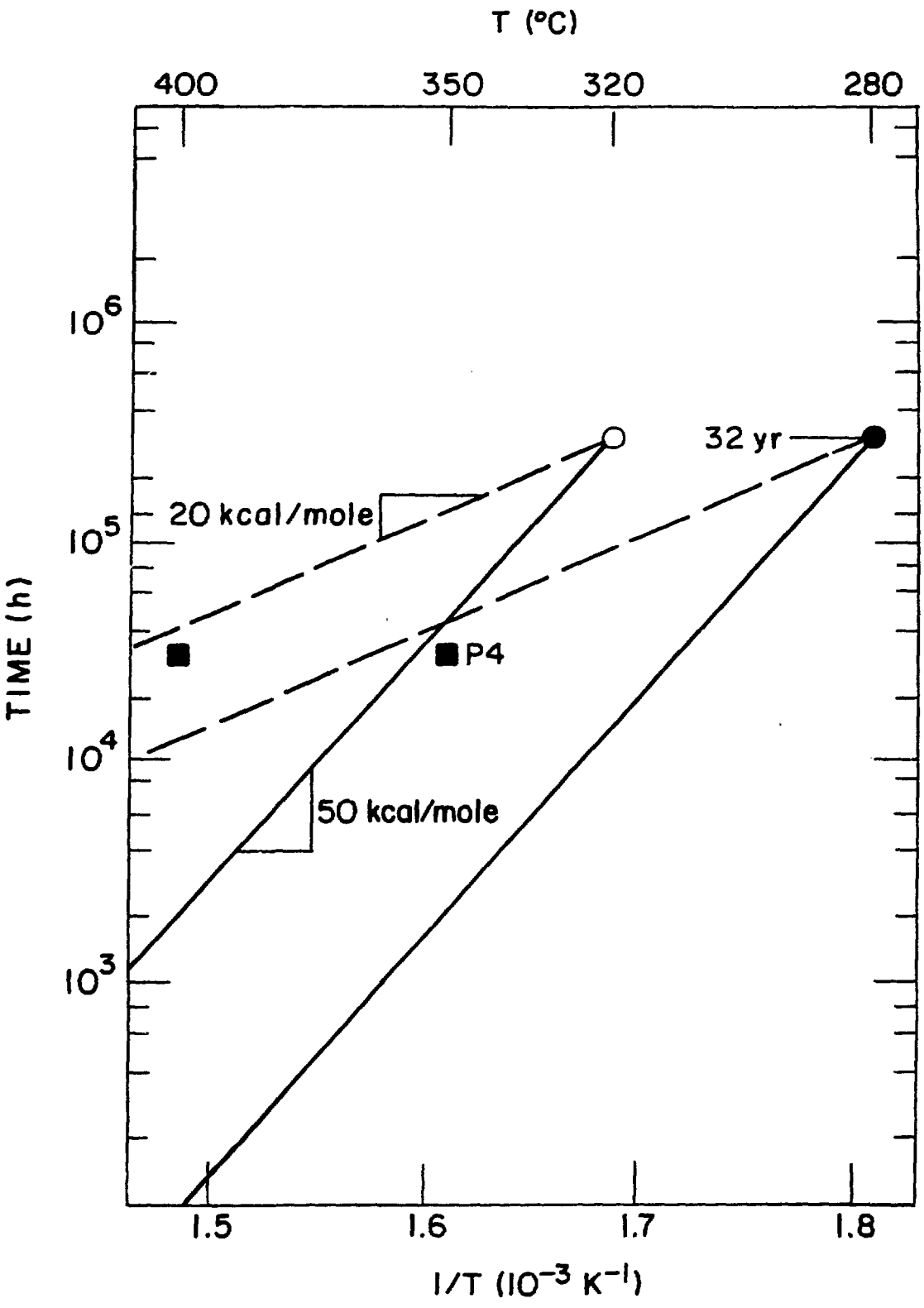
T (°C)
400
350
320
280
10^6
10^5
10^4
10^3
TIME (h)
32 yr
20 kcal/mole
P4
50 kcal/mole
1.5
1.6
1.7
1.8
1/T (10^{-3} K^{-1})